JOURNAL

OF THE AMERICAN CHEMICAL SOCIETY

VOLUME 106, NUMBER 7 APRIL 4, 1984

Polymerized Surfactant Vesicles: Kinetics and Mechanism of Photopolymerization

Wayne Reed, Lee Guterman, Piero Tundo,[1] and Janos H. Fendler*

Contribution from the Department of Chemistry and Institute of Colloid and Surface Chemistry, Clarkson College of Technology, Potsdam, New York 13676. *Received June 30, 1983*

Abstract: Formation of vesicles, prepared from styrene-containing surfactants $[H_2C{=}CHC_6H_4NHCO_2(CH_2)_{10}][C_{16}H_{33}]N^+[CH_3]_2,Br^-$ (**1**) and $[n\text{-}C_{15}H_{31}CO_2(CH_2)_2]_2N^+[CH_3][CH_2C_6H_4CH{=}CH_2],Cl^-$ (**2**), has been verified by static and dynamic light scattering and electron microscopy. Hydrodynamic diameters, D_H, of vesicles **1** and **2** decreased with increasing sonication times to plateau values of 2100 and 1450 Å. Vesicles prepared from **1** proved to be unstable on standing for a few hours, whereas those made from **2** remained stable for weeks. Weight-averaged molecular weights of vesicles prepared from **2** were determined to be 1.0×10^8 g/mol. Irradiation of **2** in ethanol or in vesicular form by a 450-W Xe lamp or by 15-ns bursts of 266-nm laser pulses at an energy of 0.1–2.0 mJ/pulse led to the disappearance of styrene absorbances. Rates of monomer disappearances were considerably slower in ethanol than in vesicles. Polymerization rates for vesicular **2** were found to be independent of vesicle concentration but depended linearly on the applied laser energy. Conversely, rates in ethanol depended on the concentration of monomeric **2**. Transient absorption spectra for **2** in ethanol and in vesicles, determined by laser flash photolysis, indicated the formation of styrene triplets (300 nm in EtOH and 320 nm in vesicles) and ground-state depletion at 250 nm. The time dependence of ground-state depletion was related to radical formation and propagation. Free-radical lifetimes and propagation times were assessed to be 17 ms ± 37% and 1 ms ± 62%, respectively. Time-resolved fluorescence anisotropies indicated a much faster rotation of **2** in ethanol (0.3 ns) than in vesicles (0.97 ns). Upon polymerization the styrene groups in vesicles lost all rotational mobility. These experimental data for vesicle photopolymerization have been accounted for in terms of a model which considers intravesicular surface reactions. In addition to correctly describing vesicle polymerization behavior, the model also provides an experimentally measurable quantity which relates average polymer chain length (determined to be 20 ± 30% monomers/chain) to the quantum efficiency of free-radical formation and other easily obtainable parameters.

Introduction

Membranes perform a variety of biological functions,[2] yet their organizational properties and utilities remain too complex to interpret, let alone to reproduce. Development of relatively simple synthetic membrane analogues has been prompted by the need to circumvent the inherent complexities of the biological ensemble.[3] Liposomes and vesicles, smectic mesophases of closed phospholipid and synthetic surfactant bilayers with interspaced water, have been used most fruitfully as membrane analogues.[4,5] Recognizing the need for enhanced stabilities, controllable permeabilities, and sizes led to the syntheses of polymerized surfactant vesicles.[6-34] Vesicle-forming surfactants have been functionalized with vinyl,[9-11] carbene,[12-14] nitrene,[12-14] methacrylate,[15-17] and diacetylene

(1) Present address: Istituto Di Chimica Organica, Della Universita de Torino, 10125 Torino, Via Bidone, 36, Italy.
(2) Martonosi, A. "Membranes and Transport"; Plenum Press: New York, 1982.
(3) Fendler, J. H. "Membrane Minetic Chemistry"; Wiley-Interscience: New York, 1982.
(4) Gregoriadis, G.; Allison, A. C. "Liposomes in Biological Systems"; Kimelberg, H. K., Mayhew, E. G. *CRC Crit. Rev. Toxicol.* **1978**, *6*, 25–79. Papahadjopoulos, D. *Ann. N. Y. Acad. Sci.* **1978**, *308*, 1–468.
(5) Fendler, J. H. *Acc. Chem. Res.* **1980**, *13*, 7–13.
(6) Gros, L.; Ringsdorf, H.; Schupp, H. *Angew. Chem., Int. Ed. Engl.* **1981**, *20*, 305–325.
(7) Fendler, J. H. In "Surfactants in Solution"; Mittal, K. L.; Lindman, B. Ed., Plenum Press: New York, 1983.
(8) Fendler, J. H.; Tundo, P. *Acc. Chem. Res.* **1983**.
(9) Kunitake, T.; Nakashima, N.; Takarabe, K.; Nagai, M.; Tsuge, A.; Yanagi, H. *J. Am. Chem. Soc.* **1981**, *103*, 5945–5947.
(10) Tundo, P.; Kippenberger, D. J.; Klahn, P. L.; Prieto, N. E.; Jao, T. C.; Fendler, J. H. *J. Am. Chem. Soc.* **1982**, *104*, 456–461.
(11) Tundo, P.; Kurihara, K.; Kippenberger, D. J.; Politi, M.; Fendler, J. H. *Angew. Chem., Int. Ed. Engl.* **1982**, *21*, 81–82.
(12) Tundo, P.; Kippenberger, D. J.; Politi, M. J.; Klahn, P.; Fendler, J. H. *J. Am. Chem. Soc.* **1982**, *104*, 5352–5358.
(13) Kippenberger, D. J.; Rosenquist, K.; Odberg, L.; Tundo, P.; Fendler, J. H. *J. Am. Chem. Soc.* **1983**, *105*, 1129–1135.
(14) Gupta, C.; Radhakrishnan, R.; Gerber, G. F., Olsen, W. L.; Quay, S.; Khorana, H. G. *Proc. Natl. Acad. U.S.A.* **1979**, *76*, 2595–2599
(15) Curatolo, W.; Radhakrishman, R.; Gupta, C. M.; Khorana, H. G. *Biochemistry* **1981**, *20*, 1374–3397.
(16) Radhakrishman, R.; Costello, C. E.; Khorana, H. G. *J. Am. Chem. Soc.* **1982**, *104*, 339–3947.
(17) Regen, S. L.; Czech, B.; Singh, A. *J. Am. Chem. Soc.* **1980**, *102*, 6638–6940.
(18) Regen, S. L.; Singh, A.; Dehure, G.; Singh, M. *Biochem. Biophys. Res. Commun.* **1981**, *101*, 131–136.
(19) Regen, S. L.; Singh, A.; Oehme, G.; Singh, M. *J. Am. Chem. Soc.* **1982**, *104*, 791–794.
(20) Tiecke, B.; Wegner, G.; Naegele, D.; Ringsdorf, H. *Angew. Chem., Int. Ed. Engl.* **1976**, *15*, 764–765.
(21) Barraud, A.; Rosilio, C.; Ruaudel-Teixier, A. *J. Colloid Interface Sci.* **1977**, *62*, 509–563.
(22) Tieke, B.; Wegner, G. *Macromol. Chem.* **1978**, *179*, 1639–1642.
(23) Day, D.; Ringsdorf, H. *J. Polym. Sci., Polym. Lett. Ed.* **1978**, *16*, 205–210.
(24) Day, D.; Ringsdorf, H. *Makromol. Chem.* **1978**, *180*, 1059–1063.
(25) Day, D.; Lando, J. B. *Macromolecules* **1980**, *13*, 1478–1483, 1483–1487.
(26) Hupfer, B., Ringsdorf, H.; Schupp, H. *Makromol. Chem.* **1981**, *182*, 247–253.

0002-7863/84/1506-1897$01.50/0

groups.[18-34] Polymerized surfactant vesicles have potential utilization in photochemical solar energy conversion, drug delivery, and reactivity control, and in the duplication of many other membrane-mediated processes.[6-8] Exploitation of these potentials demands the full characterization of polymerized surfactant vesicles and an understanding of the kinetics and mechanisms of polymerization.[35-39]

Attention in the present report is focused upon the kinetics and mechanism of surfactant vesicle photopolymerization. Polymerized vesicles have been prepared from surfactants containing styrene groups in the end of their hydrocarbon tails or at their headgroups. The styrene moiety allowed the convenient monitoring of the polymerization by absorption spectrophotometry.[40] Steady-state and pulsed-laser irradiations provided the ultraviolet photons for the polymerization. Vesicle molecular weights and sizes have been determined by steady-state[41,42] and dynamic[43-45] light scattering, respectively. A theoretical model for surfactant vesicle photopolymerization has been developed. This model treats the kinetics in terms of free-radical formation, polymer-chain propagation, radical deactivation, and chain termination and allows an approximation of the degree of polymerization. Determinations of the rates of surfactant vesicle photopolymerization as functions of the amounts and intensity of absorbed energy, vesicle concentrations and sizes, and presence or absence of oxygen have provided experimental support for the proposed model. Studies involving flash photolysis and fluorescence anisotropy have provided a quantitative basis for elaborating the proposed theory for the photopolymerization of surfactant vesicles.

Experimental Section

Preparation, purification, and characterization of monomeric surfactant $[H_2C{=}CHC_6H_4NHCO_2(CH_2)_{10}][C_{16}H_{33}]N^+[CH_3]_2Br^-$ (**1**) have been previously described.[8] $[n\text{-}C_{15}H_{31}CO_2(CH_2)_2]_2N^+[CH_3][CH_2C_6H_4CH{=}CH_2],Cl^-$ (**2**)[12] was synthesized by heating 1.79 g (3 mmol) of bis[2-(*n*-hexadecanoyloxycarbonyl)ethyl]methalmine, 0.92 g (6 mmol) of vinylbenzyl chloride (Fluka, mixture of isomers), and 0.1 g (2 mmol) *tert*-butylcatechol for 24 h at 60 °C. Purification of the reaction mixture on a silica gel column (using $CHCl_3$ and MeOH:$CHCl_3$ = 90:10, v/v, successively as eluents) gave 1.32 g of **2** (52% yield), mp = 61–65 °C (recryst CH_3CN): ^1H NMR ($CDCl_3$ δ 7.25–7.85 (m, 4 H aromatic), 5.20–5.95 and 6.50–7.00 (m, 3 H vinyl), 5.15 (br s, 2 H), 4.68 (br t, 4 H), 4.08 (br t, 4 H), 3.35 (s, 3 H), 2.35 (br t, 4 H), 1.0–1.8 (br s, 52 H), 0.88 (t, 6 H).

Deionized water was doubly distilled in an all-glass apparatus. The final stage of distillation included a superheated oxygenated quartz column. Doubly distilled water was filtered through a 0.2-μ Millistak (Millipore Corp.) filter to provide dustless water.

Glassware was cleaned by consecutively soaking and rinsing in concentrated H_2SO_4, water, 0.02 M $KMnO_4$ in 2.0 M NaOH, water, 5.0×10^{-3} M $NH_2OH{\cdot}HCl$ in 2.0 M HCl, water, singly distilled water (six rinses), dustless water (three rinses). Clean glassware was wrapped in foil and dried at 80 °C.

Vesicles were prepared by sonication using the microtip of a Braunsonic 1510 sonicator set at 70 W. Typically, appropriate amounts of solid **1** and **2** were weighed and placed into a 25-mL test tube to give 1.7×10^{-4} M **1** and 7.0×10^{-4} M **2** upon the addition of 20 mL of doubly distilled water. The test tubes, capped with rubber diaphragms, were placed into a thermostat (set for 65 °C for **1** and 75 °C for **2**) for 30 min prior to sonication. Dispersal of the surfactant was facilitated by occasional vortexing. Incubated samples were sonicated at the appropriate temperature for times ranging from <1 min to 60 min (see Results). Sonicated samples were ultrafiltered through an Amicon MMC unit (Diaflow YM series membranes) and subsequently through Nucleopore polycarbonate membranes (ranging in size from 0.1 to 1.0 μm). Membranes, used in both filtrations, were routinely presoaked in doubly distilled dustless water.

Vesicle polymerizations were carried out on samples degassed by gently bubbling argon, passed through a water trap, for several hours (typically overnight). A 450-W xenon lamp (Oriel Corp.) was used for steady-state irradiations. Infrared radiation was removed by placing water, in a 2.5 × 2.5 cm quartz cell, at the exit port of the lamp house. The xenon lamp beam was focused on the cell so that the entire volume was under constant irradiation. The irradiation cell was placed 35 cm from the light beam. The intensity of the radiation in the range of 240–350 nm was calculated from Oriel's specifications to be less than 3.33 mW/cm^2, which corresponds to a photon flux of less than 4.46×10^{15} photons/cm^2. For laser-initiated vesicle photopolymerization studies, pulsed monochromatic ultraviolet photons were provided by a Quanta Ray DCR 1A Nd:YAG laser. Three modes of pulse input were available: single shot, 2 Hz, and 10 Hz. Laser intensities were measured by a Scientech 362 power meter. Thermostated vesicles were bubbled with purified argon during both the steady-state and the laser photolysis. Additional stirring for the steady-state photolysis was provided by a magnetic stirrer. The progress of photopolymerization was followed by determining the absorption spectra for 300-μL aliquots taken from the sample at appropriate time intervals for the steady-state irradiation and by examining the entire sample for laser-initiated polymerizations. Logarithms of absorbances at 250 nm at different times were plotted as a function of irradiation time (steady state) and as a function of laser energy (laser photopolymerization).

Freeze-dried vesicles were used for **polymer fragment analysis**. The method involved a comparison between polymerized and nonpolymerized vesicles. Typically, an 80-mL batch of vesicle was divided into two portions; one was polymerized, one was not. Both aliquots were freeze-dried on a Labconco 75200 Missouri freeze drier. Separately weighed portions of the freeze-dried samples (polymerized vesicle and its nonpolymerized control) were dissolved in water, ethanol, methanol, methylene chloride, dichloroethylene, and tetrahydrofuran and light scattered, in turn.

Steady-state light scatterings were performed on a Brice-Phoenix light scattering photometer at 25 °C. A 20-mL square quartz cell was used for 90° scattering, whereas a cylindrical cell of the same volume was employed for angular studies. Scrupulous cell cleaning and preparation of dust-free samples were found to be mandatory. A Brice-Phoenix differential refractometer was used for measuring changes in the refractive index increment. NBS standard samples of polystyrene were used to verify the calibration of the light-scattering equipment. Software has been developed for the computer treatment of static light-scattering data for obtaining $\bar{M}_w$ by employing Zimm diagrams.[46]

The **dynamic light scattering system** utilized an illumination source (a 12-W 171 Spectra Physics Ar^+ ion laser), a goniometer, and digital correlator–microprocessor (Brookhaven Instrument). Prior to collecting dynamic light-scattering data, the count rate was established for the refractive index matched quartz sample holder dish in the goniometer. Acceptable levels never exceeded 0.25% of sample count rate. Cleaned rinsed cells were placed in a steam jet. If no condensation formed, and the steam rolled off in a continuous sheet, the cell was deemed clean. It was then filled with dustless H_2O and the scattering intensity was measured. For surfactant vesicles, typically 10^7 total counts were accumulated over a 300–600-μs time window. Since the surfactant concentration in vesicle solutions never exceeded 0.05% weight, the viscosity and refractive index of solvent (H_2O) were taken for the values of vesicle solutions. Quality factors, describing deviations of the data from monodispersity, were always less than 0.4. Hydrodynamic radii with higher Q values were attributed to cell spots or dust. Monitoring the magnitude of scattering count was imperative. Excessive counts resulted in pre-

(27) Koch, H.; Ringsdorf, H. *Macromol. Chem.* **1981**, *182*, 255–259.
(28) Hub, H. H.; Hupfer, B.; Koch, H.; Ringsdorf, H. *J. Macromol. Sci., Chem.* **1981**, *15*, 701–715.
(29) Albrecht, O.; Johnson, D. S.; Villaverole, C.; Chapman, D. *Biochem. Biophys. Acta* **1982**, *687*, 165–171.
(30) Johnson, D. J.; Sanghera, J.; Pons, M.; Chapman, D. *Biochem. Biophys. Acta* **1980**, *602*, 57–69.
(31) O'Brien, D. F.; Whitesides, T. H.; Klingbiel, R. T. *J. Polym. Sci., Polym. Lett.* Ed. **1981**, *19*, 95–101.
(32) Lopez, E.; O'Brien, D. F.; Whitesides, T. H. *J. Am. Chem. Soc.* **1982**, *104*, 305–307.
(33) Bader, H.; Ringsdorf, H. *J. Polym. Sci., Polym. Chem.* Ed. **1982**, *20*, 1623–1628.
(34) Day, D.; Hub, H. H.; Ringsdorf, H. *Isr. J. Chem.* **1978**, *18*, 325–329.
(35) Paleous, C. M.; Dias, P. *J. Polym. Sci., Polym. Chem. Ed.* **1978**, *16*, 1495–1503.
(36) Paleus, C. M.; Christias. C.; Evangelatos, G. P.; Dais, P. *J. Polym. Sci., Polym. Chem. Ed.* **1982**, *20*, 2565–2573.
(37) Norrish, R. G. W.; Simons, J. P. *J. Chem. Soc.* **1958**, 4–26.
(38) Lichti, G.; Sangster, D. F.; Whang, B. C. Y.; Nappes, D. H.; Gilbert, R. G. *J. Chem. Soc., Faraday Trans. 1* **1982**, 2129–2145.
(39) Mayoral, J.; Levy, M. *J. Polym. Sci., Polym. Chem.* Ed. **1982**, *20*, 2755–2764.
(40) Kauffmann, H. F. *Makromol. Chem.* **1979**, *180*, 2649–2663.
(41) Hiemenz, P. C. "Principles of Colloid and Surface Chemistry"; Marcel Dekker: New York, 1977.
(42) Kratohvil, J. P.; Smart, C. *J. Colloid Sci.* **1965**, *20*, 875–892.
(43) Berne, B. J.; Pecora, R. "Dynamic Light Scattering"; Wiley: New York, 1976.
(44) Pusey, P. N. In "Proton Correlation and Light Beating Spectroscopy", Cummins, H. T., Pike, E. K., Eds.; Plenum Press: New York, 1974.
(45) Chu, B. "Laser Light Scattering"; Academic Press: New York, 1974.
(46) Reed, W. unpublished results, 1983.

mature buildup of the autocorrelation function, and hence valuable intensity fluctuations were lost. Large fluctuations in intensity implied multimodal population and/or dust. Utilizing an Ortec Model 776 counter and timer, small fluctuations in intensity were monitored. The signal-to-background ratio was maximized by employing the smallest possible slit preceding the PM tube. The goniometer output was connected to a Model M2000 Digital correlator. This entirely digital 64-channel high-speed signal processor operates in real time. Its basic function is to digitally construct the autocorrelation function through a series of shift registers, multipliers, and accumulators acting on the incoming, fluctuating intensity signal from the PM tube. The 64 channels could be manipulated to cover various sample times ranging from 100 ns–900 ms. Basically, this procedure varies a time window, facilitating selective sampling of particular components of the population. In addition, the experimental duration could also be controlled (i.e., total number of samples collected over 1 to 9000 s). Duration time was commonly 200 s which produced 10^7 counts. To examine 1500-Å vesicles in H_2O, full decay of the autocorrelation function over the entire 64 channels was achieved at 10 μs/channel.

Flash photolysis measurements were carried out using the fourth harmonic (λ = 266 nm) of a Nd:YAG laser (Quanta Ray DCR-1A) for excitation, and a xenon lamp (150 W Oriel) for the analyzing light. A manual trigger provided the start signal for opening a fast shutter between the xenon lamp and sample cell, triggering the fast digitizer (Tektronix RF912), and dropping the electro-optical Q switch in the laser cavity to zero potential, thus firing the laser. An adjustable delay box allowed the time between digitizer triggering and laser firing to be selected so that the prelaser-pulse light level transmitted through the sample appeared on the waveform as well as the succeeding laser-induced events. The pulse of 15 ns fwhm was used at an energy level of approximately 10 mJ/pulse as measured by a Scientech disc power meter (36-2002) operating as a surface absorber, rather than as a volume absorber. An optical train of ultraviolet transmitting lenses focused the collimated xenon lamp light into the sample cell and refocused the transmitted light onto the entrance slit of a Jarrell-Ash 25-cm monochromator equipped with low blaze for ultraviolet measurements. A Hammamatsu R928 phototube was used for measuring the light level transmitted through the sample cell. The phototube divider network used a short five-dynode plan for fast response and artifact-free operations. The Tektronic digitizer was interfaced to a DEC PDP11/34A minicomputer. The minicomputer controlled the digitizer. Software has been developed for signal averaging, final data reduction, analysis, and graphics. Signal averaging at 8 mJ/pulse was limited to a maximum of 15 shots per fresh sample of vesicle solution, as the sample is about 10% polymerized after about 100 mJ of energy deposition.

Fluorescence lifetime measurements were performed by using a Spectra Physics 171 mode-locked argon ion laser which synchronously pumped a Spectra Physics 375 dye laser as the excitation source. The dye laser cavity energy is output coupled by means of a radio-frequency modulated Bragg diffraction cell which allowed cavity dumping at selected frequencies up to 4 MHz. A birefringent intracavity filter tuned the laser between 550 and 620 nm. For excitation of the styrene moieities, the cavity-dumped dye laser output was frequency doubled with an Inrad ADA temperature-controlled crystal to provide excitation at 296 nm. A portion of the undoubled dye output provided the start signal for the ORTEC 457 time-to-amplitude converter (TAC). The stop signal was provided by the first fluorescence photon emitted from the excited sample detected by an RCA 8050 PM tube. A neutral density filter was placed before the sample to attenuate excitation to the point where 5% of the pulses yielded single detected fluorescence photons, and a tiny percent led to multiple fluorescence photons. These statistics implied that the majority of detected events came from single fluorescence photons. The TAC output for each event, a voltage proportional to the time delay between sample excitation and detection of a single emitted photon, was sorted and accumulated by an ORTEC multichannel analyzer which builds a statistical profile of fluorescence decay behavior. The final data for the experimental $O_e(t)$ decay profile collected in 256 discrete data channels, convertible to real time, was transferred to the DEC PDP 11/34A minicomputer. Since the instrument response time has a large effect, it was necessary to deconvolute this response behavior from the decay profile $O_e(t)$. The response function, $R(t)$, is measured separately using a scattering solution in the cell compartment. The true molecular decay function, $D(t)$, is then deconvoluted from the expression:

$$O_e(t) = \int_0^t R(t - T)D(T)\,dT \qquad (1)$$

by means of a Marquadt algorithm which minimizes χ_r^2

$$\chi_r^2 = \frac{1}{256 - N}\sum_{n=1}^{256}\frac{[O_e(n) - O_c(n)]^2}{O_e(n)} \qquad (2)$$

Table I. Hydrodynamic Diameters, D_H, of Vesicles and Polymerized Vesicles Prepared from **1** and **2** under Different Conditions[a]

conditions		sampling time, μs	D_H, Å
2.0×10^{-4} M **1**	incubated at 65 °C for 10 min	50	6370
	sonicated for 5 min	10	2368
		50	7296
	sonicated for 10 min	10	2245
		50	6814
	sonicated for 20 min	10	2284
	sonicated for 30 min	10	1657
	sonicated for 10 min, filtered 0.6-μm nucleopore filter	5	1715
		10	1855
		20	1920
		50	2260
	sonicated for 10 min and allowed to stand 2 h at room temperature	10	5000[b]
	sonicated for 10 min, diluted 5-fold by H_2O, laser polymerized, Ar bubbled	10	2403
7.0×10^{-4} M **2**	sonicated for 40 min	5	1715
		10	1875
	sonicated for 1 h	5	1156
		10	1416
	sonicated for 1 h, bubbled overnight with Ar	10	1430
	sonicated for 1 h, bubbled overnight with Ar, filtered 0.6-μm nucleopore filter	10	1320
	sonicated for 1 h, bubbled overnight with Ar, filtered 0.6-μm nucleopore filter, polymerized	10	1390

[a] All measurements were takne at 90° to the incident beam, and at 25 °C, unless stated otherwise. [b] Q value is 0.96 ± 10%. On longer standing more extensive coagulation occurs.

by systematically searching the parameter space of N independent parameters (decay times, relative fractions, amplitude, time shift between reponse and decay profiles, and background noise) for a minimum χ_r^2. $O_c(n)$ refers to the calculated, reconvoluted value for the observed decay function when a trial decay function, $D(t)$, is integrated with $R(t - T)$ in eq 1.

^{1}H NMR spectra were taken on a Varian XL 200 spectrometer. All chemical shifts were assigned with respect to the $CHCl_3$ line (δ 7.24 ppm vs. Me_4Si).

Absorption spectra were taken on a Cary 118 C spectrophotometer and fluorescence spectra were obtained on a Perkin-Elmer LS-5 spectrofluorometer instrument.

Transmission electron microscopy was performed on negatively stained (3% aqueous ammonium molybdate) samples; 300-mesh Cu grids, coated with parlodium support and evaporated carbene, were prepared. A drop of the vesicle suspension was allowed to settle on the grid for 1 min and excess moisture was removed by small filter paper triangles. A drop of stain was then applied to the grid and allowed to settle for 30 s, after which the excess was removed by filter paper. Subsequent to drying for 5 min, the specimen was examined under a Phillips 201 TEM equipped with a plate camera and anticontamination device. Kodak polycontrast resin-coated paper was used to print the negatives.

Results

Preparation and Characterization of Surfactant Vesicles. Ultrasonic dispersal of surfactants **1** and **2** above their phase-transition temperatures resulted in vesicle formation. Dynamic light scattering established the hydrodynamics diameters of vesicles (Table I). Increasing the sonication times resulted in an exponential decrease of vesicle sizes and polydispersities (Table I and Figure 1). Large (D_H > 10000 Å) polydisperse aggregates formed even in the absence of sonication. Short-term sonication led to multidispersed vesicle populations (compare light-scattering data taken at different sample times). Well-sonicated samples provided relatively uniform vesicle populations. Filtration through 0.6-μm nucleopore filters further increased the unifromity.

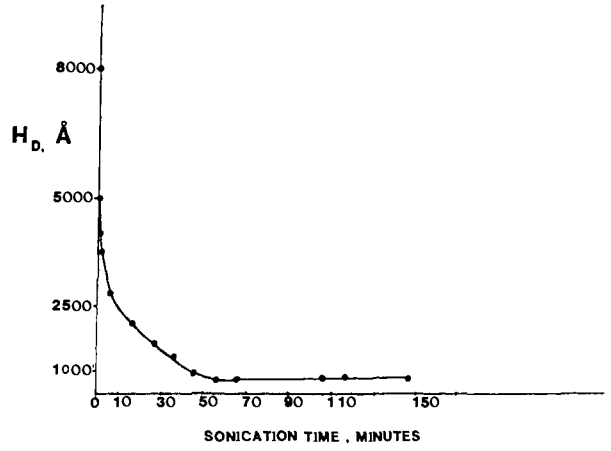

Figure 1. Plot of hydrodynamic diameters of vesicles prepared from 7.0 × 10^{-4} M stoichiometric **2** at 75 °C as a function of sonication time.

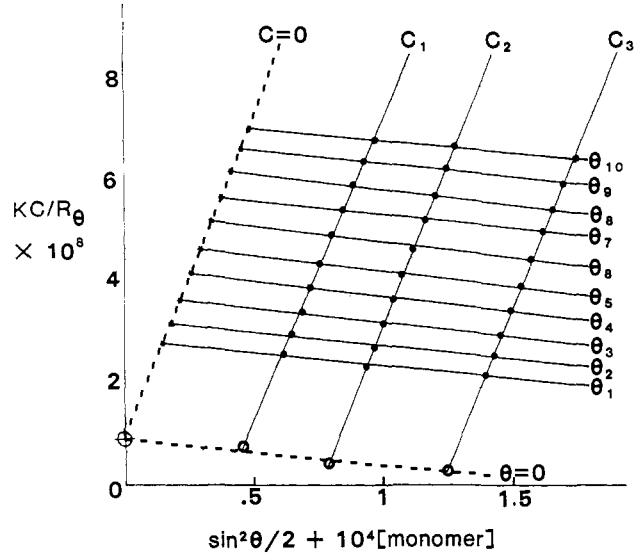

Figure 2. Zimm plot for the determination of $\bar{M}_w$ for vesicles prepared from **2** (D_H = 1500 Å from dynamic light scattering). C_1 = 4.76 × 10^{-5} g/cm³; 6.33 × 10^{-5} M. C_2 = 7.893 × 10^{-5} g/cm³; 1.05 × 10^{-4} M. C_3 = 1.25 × 10^{-4} g/cm³; 1.67 × 10^{-4} M. θ_1 = 45°; >θ_2 = 50°; θ_3 = 55°; θ_4 = 60°; θ_5 = 65°; θ_6 = 70°; θ_7 = 75°; θ_8 = 80°; θ_9 = 85°; θ_{10} = 90°; M_w = 1.1561 × 10^8 ± 6%.

Vesicles prepared from **1** underwent spontaneous growth and ultimately precipitated. On the other hand, vesicles prepared from **2** had long term stabilities. Overnight bubbling by Ar and standing for a week did not alter their hydrodynamic diameters (Table I). All detailed investigations were limited, therefore, to vesicles prepared from **2**.

Weight-averaged molecular weights, $\bar{M}_w$, of vesicles prepared from **2** were determined by static light scattering using the equation:[41,42]

$$\frac{KC}{R_\theta} = \left(\frac{1}{\bar{M}_w} + 2BC\right)\left(1 + \frac{16\pi^2 R_G^2}{3\lambda}\sin^2\frac{\theta}{2}\right) \quad (3)$$

where C is the concentration in g/mL, B is the second virial coefficient, R_G is the radius of gyration, R_θ (the Rayleigh ratio) is the relative intensity of the scattered light, λ is the wavelength of excitation, and K is given by:

$$K = (2\pi^2 n^2/\lambda^4 N_A)(dn/dc)^2(1 + \cos^2\theta) \quad (4)$$

where n is the refractive index, dn/dc is the refractive index increment, and N_A is Avogadro's number. Plots of the left-hand side of eq 3 against 10^4-C + $\sin^2\theta/2$ at different stoichiometric surfactant concentrations and different detection angles lead to a family of straight lines, generally depicted as a Zimm plot (Figure 2). Extrapolation to zero concentration and zero angle led to a value of $\bar{M}_w$ = 1.05 × 10^8 ± 6% and 1.05 × 10^8 ± 24%, respectively (with a 0.999 correlation coefficient), for surfactant vesicles prepared from **2**. Since the molecular weight of monomeric **2** is 750, each vesicle contains 1.4 × 10^5 surfactant monomers. For vesicles with 1500-Å diameters, we obtain surface areas of 94 Å² occupied per monomer,[47] which agrees well with literature values.[3] These geometric calculations substantiate our assumption that the vesicles are single-compartment bilayer structures. Assuming the vesicles to contain two sets of bilayers, separated by a 50-Å water layer, would lead to an unrealistically high surface area of 164 Å² per monomer.[48] Furthermore, the presence of surfactant clumps, rather than single lamellar bilayer vesicles, would require 50 times more monomers per 1500-Å D_H vesicles. These values are considerably outside our experimental errors and strongly support the existence of unilamellar bilayer vesicles.

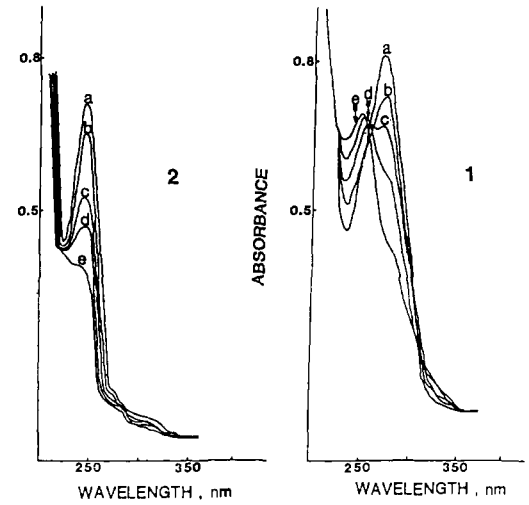

Figure 3. Absorption spectra of vesicles prepared from 3 × 10^{-5} M stoichiometric **1** (D_H = 2400 Å from dynamic light scattering) prior (a) and subsequent to irradiation by 200 (b), 700 (c), 1700 (d), 4800 (e) mJ of laser power; and those prepared from 1.4 × 10^{-4} M **2** (D_H = 1400 Å from dynamic light scattering) prior (a) and subsequent to irradiation by 140 (b), 600 (c), 1000 (d), and 3000 (e) mJ of laser power.

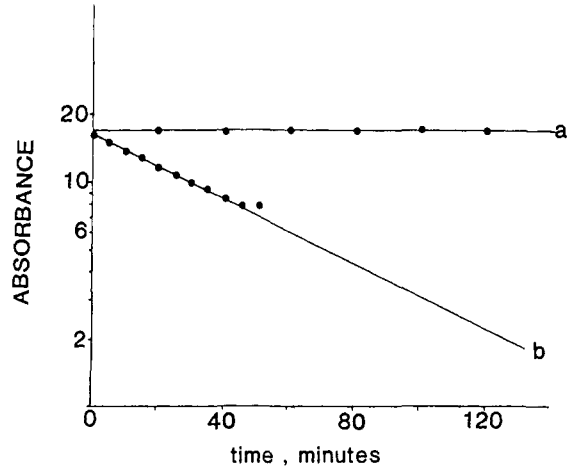

Figure 4. Monomer conversion rates of vesicles prepared from 1.4 × 10^{-4} M **2** (a) and those of a 7.0 × 10^{-4} M ethanolic solutions of **2** (b) as functions of irradiation time using a 450-W xenon lamp.

(47) Assuming an outside radius of 750 Å and 50-Å bilayer thickness leads to surface areas of 7.065 × 10^6 Å² for the outer (A_o) and 6.154 × 10^6 Å² for the inner A_i) surface. The total surface area $A_t = A_o + A_i$ = 1.322 × 10^7 Å². Hence the surface area per monomer is A_t/M_w of vesicle/M_w of monomer = 1.322 × 10^7 Å²/1.052 × 10^8 1750 = 94 Å².

(48) Surface area of the outer bilayer A_t^I = 1.32 × 10^7 Å², surface area of the inner bilayer, A_t^{II}, assuming 650 and 600 Å for the outer and inner radii, respectively, is 9.828 × 10^6 Å. Hence the total surface area of the two bilayers are = $A_T = A_t^I + A_t^{II}$ = 2.305 × 10^7 Å². Hence the surface area per monomer is = A_T/M_w of monomer = 2.305 × 10^7 Å²/1.052 × 10^8 1750 = 164 Å².

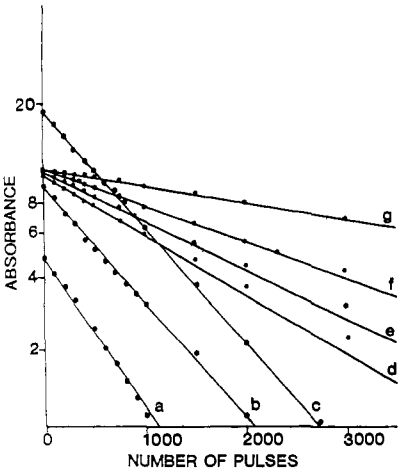

Figure 5. Plotted are log absorbances at 250 nm for vesicles prepared from **2** vs. number of laser pulses at 1 mJ/pulse unless stated otherwise: (a) 7.0×10^{-6} M, (b) 1.4×10^{-5} M, (c) 1.4×10^{-4} M, (d) 1.4×10^{-4} M, all at 0.60 mJ/pulse, (e) 1.4×10^{-4} M at 0.50 mJ/pulse, (f) 1.4×10^{-4} M at 0.35 m/J pulse, and (g) 1.4×10^{-4} M at 0.15 mJ/pulse.

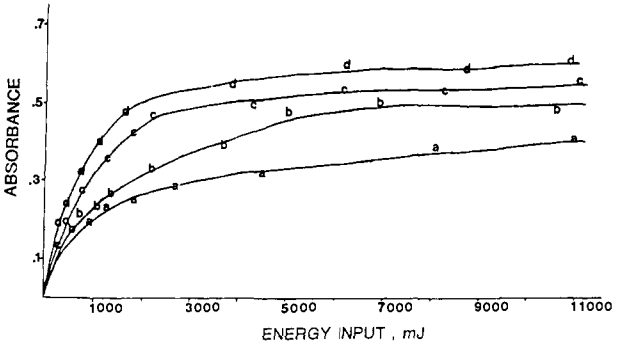

Figure 6. Plots of absorbances due to photoproduct buildup at 325 nm of monomer conversion for ethanolic 5.76×10^{-7} M (a), 1.0×10^{-6} (b), 2.5×10^{-5} M (c), and 5.0×10^{-5} M (d) **2** as functions of laser energy. Lines were normalized to the same absorption cross section.

Absorption spectra of vesicles prepared from **2** show characteristic bands due to the styrene moiety at 266 nm with an extinction coefficient of 1.6×10^3 M^{-1} cm^{-1}. For the sake of comparison, the absorption spectra of **2** were also determined in ethanol. In this solvent $\epsilon_{266nm} = 9 \times 10^3$ M^{-1} cm^{-1}.

Kinetics of Polymerization. Irradiation of vesicles prepared from **2** by a 450-W xenon lamp resulted in the exponential loss of the absorbance due to styrene moiety (Figure 3), presumably due to polymerization. The rate of loss of absorbance was found to be appreciably faster for vesicles than for alcoholic solutions of **2** (Figure 4). Good reproducibility of absorption changes were found from kinetic run to run.

Irradiation of vesicles prepared from **2** by pulsed 266-nm laser light also resulted in the exponential loss of absorbance due to styrene as a function of absorbed laser energy (Figure 5). Advantages of laser irradiation are the monochromatic light and the high and controllable intensity of radiation. Increasing the laser intensity led to faster polymerizations (Figure 5). Changes in vesicle concentration did not affect the polymerization rate.

Sizes of vesicles were not found to be altered upon their polymerization (Table I). Monomeric **2** was dissolved in ethanol at concentrations ranging from 10^{-7} to 10^{-4} M. If the loss of monomer absorption in EtOH had been first order, i.e., the monomers were merely being photolyzed, the absorption vs. energy curves would have been equal when scaled to the same concentration. In fact, kinetic data indicated a multi-order concentration-dependent function describing monomer disappearance in bulk that required four times as much laser energy to achieve half the conversion found in vesicular solutions (see Figure 6).

Steady-State and Nanosecond Time-Resolved Fluorescence. Excitation of surfactant vesicles prepared from 2.0×10^{-4} M **2** resulted in an emission spectra with maxima at 347 and 415 nm (Figur e 7) presumably due to fluorescing monomers and excimers. Similar fluorescence behavior was observed in an ethanolic solution of **2**. These spectra are entirely analogous to those observed for styrene.[37] Fluorescence spectra of vesicles prepared from **2** subsequent to laser irradiation showed the expected trend: the decrease of the monomer to excimer ratio (Figure 7).

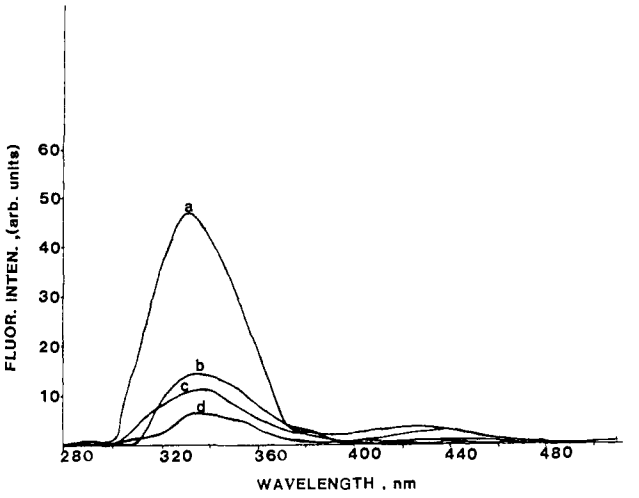

Figure 7. Fluorescence spectra of vesicles prepared from 1.4×10^{-4} M **2** at different monomer conversions; λ_{ex} 266 nm. Pulsed laser irradiations utilized 0 (a), 450 (b), 4500 (c), and 7500 mJ (d) of energy.

Table II. Fluorescence Lifetimes, τ, and Anisotropies, τ_R, of **2** in Different Environments[a]

	λ_{obsd}, nm	F_1, %	τ_1, ns	F_2, %	τ_2, ns	τ_R,[b] ns
unpolymerized	347	45	0.25	55	6.1	0.97 + 0.19
vesicles of **2** (D_H = 2000 Å)	410	8	0.30	92	4.5	>>10
laser-polymerized	347	signal is too weak				
vesicles of **2** (D_H = 2000 Å)	410	<7	0.40	>97	4.5	>>10
2×10^{-5} M **2** in	350	11	1.43	89	5.28	0.3 ± 0.04
EtOH	448	52	3.2	48	8.74	

[a] Fluorescence lifetimes and fractions F are accurate to 10 and 15%, respectively, for one confidence interval. [b] τ_R calculated from equation 5, taking $G = 1.24 + 0.05$, determined by tail-matching $I_{(\parallel)}$ and $I_{(\perp)}$ curves for 2 in EtOH where complete rotational reorientation is assumed for long times (>10 ns).

2 in ethanol showed multiexponential fluorescence lifetimes which at any wavelength could be resolved reasonably well ($\chi^2 < 2.5$) into two lifetimes. Table II summarizes the single photon counting data. In ethanol the shorter lifetimes probably originate from monomer emission while the longer ones are due to aggregates. Light-scattering data support the association of some fraction of **2** in ethanol at the concentrations employed. In vesicles, prepared from **2**, the fast decay, which predominates at 347 nm with a lifetime of ca. 0.25 ns, is due to monomer emission, while the slower decay, predominating at the longer wavelength with a lifetime of ca. 4.5 ns, is attributable to excimer emission. Upon polymerization the short lifetime is almost entirely lost; the residual emission signal at 347 nm is too weak to measure. The signal at 410 nm observed in polymerized vesicles was found to be of considerably greater intensity. It decayed with a single lifetime of 4.5 ns.

Figure 8 shows plots of the polarization anisotropy function $A(t)$ where

$$A(t) = \frac{GI_{(\parallel)} - I_{(\perp)}}{GI_{(\parallel)} + 2I_{(\perp)}} = Ae^{-t/\tau_R} \qquad (5)$$

$I_{(\parallel)}$ and $I_{(\perp)}$ are time-dependent fluorescence intensities observed through polarizers oriented parallel and perpendicularly to the vertically polarized excitation, τ_R is the rotational correlation time,

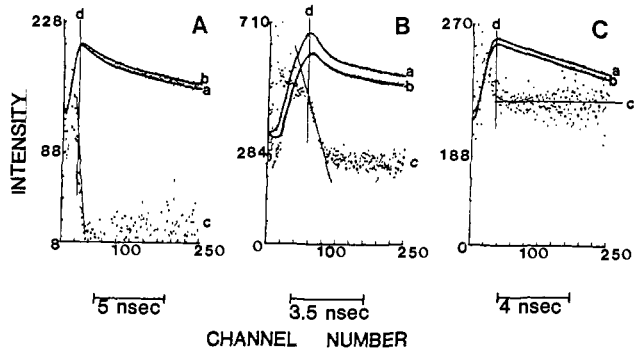

Figure 8. Time-dependent fluorescence anisotropies of 1.4×10^{-4} M ethanolic **2** (A) and of vesicles prepared from 1.4×10^{-4} M **2** prior (B) and subsequent (C) to laser photopolymerization. Plotted are the lifetimes observed parallel (a) and perpendicular (b) to the vertical laser excitation. Also shown are the plots of the anisotropy values, $A(t)$ vs. time, according to eq 5 (c). Line d indicates the first channel the lifetime was taken.

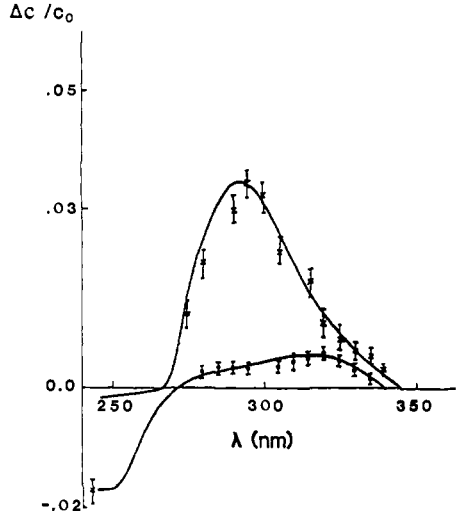

Figure 9. Transient absorption spectra of 1.4×10^{-4} M **2** in ethanol (top curve) (×) and of vesicles prepared from 1.4×10^{-4} M **2** (●).

and G is a system-dependent optical correction factor. **2** in ethanol underwent complete rotational relaxation in ca. 0.3 ns as determined from the monomer emission at 350 nm. In contrast, the fluorescence signal at 340 nm in unpolymerized **2** vesicles indicated a τ_R value of ca. 1 ns. Rotation of the styrene group in vesicles is evidently hindered. There is an incomplete decay of the anisotropy, $A(t)$, which remains at 0.25 after the initial 1-ns rotational relaxation (Figure 8). This indicates incomplete reorientation of the styrene moiety. Complete reorientation of the last remaining degree(s) of rotational freedom would presumably require the complete rotational reorientation of the entire vesicle. Measuring the anisotropy at 410 nm gave a small initial decay of ca. 1 ns. This is due to the presence of some (ca. 8%) of monomer emission at this wavelength. Subsequent to polymerization the unassociated monomer signal is not apparent at any wavelength, and the emission signal at 410 nm yields a constant $A(t)$ value (Figure 8). Apparently the large freely rotating population of unassociated monomeric **2** becomes liked and hence rotationally immobile upon polymerization.

Laser Flash Photolysis. The laser flash photolysis data gave quantitative insight into vesicle photopolymerization. It allowed the experimental estimation of the kinetic parameters used in mechanistic treatment of vesicle polymerization (see Discussion) and provided values for the quantum efficiency and rate constants for free-radical formation.

Transient spectra of **2** in EtOH and in the forms of vesicles are shown in Figure 9 immediately after excitation by a 15-ns laser pulse. Salient features are the broad absorptions, with maxima at 300 nm in EtOH and 320 nm in vesicles, and

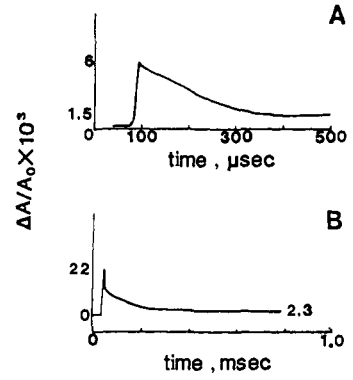

Figure 10. Decay of transient absorbancies (Ar bubbled) due to triplets formed from vesicles prepared from 1.4×10^{-4} M **2**, observed at 320 nm (A) and that from 1.4×10^{-4} M **2** in ethanol, observed at 300 nm (B). Digitized decay of the average of 10 shots are shown.

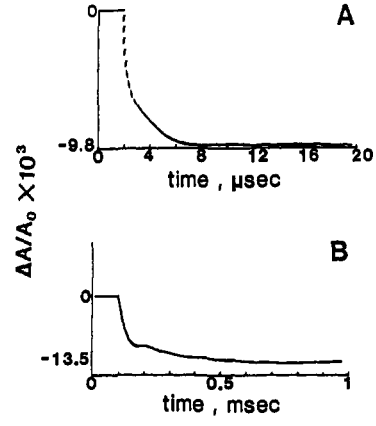

Figure 11. Depletion of the monomer signal, observed at 250 nm, for vesicles prepared from 1.4×10^{-4} M **2** at different observation time scales. Digitized traces of the average of 10 shots are shown.

ground-state bleaching. The amount of triplet formed is substantially less and the extent of ground-state bleaching is considerably greater for **2** vesicles than for ethanolic solutions of **2**.

Triplet decays are shown in Figure 10. In ethanol the decay could be resolved into a fast component with a lifetime of ca. 5 μs and a slow component with a lifetime of ca. 200 μs. Decay of the triplet in vesicles prepared from **2** occurs on the 0.5-ms time scale. The fast component, if it exists, could not be resolved, though this may be an instrumental limitation. Upon bubbling oxygen the triplet signal is greatly diminished.

Figures 11A and 11B show the transient depletion of the 250-nm absorbance following the laser pulse on a shorter (20 μs full scale) and on a longer (1 msec full scale) time scale for **2** vesicles. Figure 11A was obtained by subtracting the computer-averaged fluorescence-scattering profile (8–10 puses without analyzing light) from the similarly averaged transient depletion (10 pulses with analyzing light). The short-time build-down shown in Figure 11A may well correspond to free-radical formation from the triplet. A rate constant, k_f, of ca. 2×10^5 s^{-1} was calculated for this process. The slight additional build-down of the **2** vesicle depletion signal (Figure 11B) may well represent the incipient stages of polymer chain propagation, k_p. Because of the millisecond level instabilities of the analyzing Xe lamp, the actual time course of polymerization could not be observed on longer time scales. Nevertheless, by taking a trace of the analyzing light (blocking the path of the laser) in less than 2 s subsequent to obtaining the transient depletion at 250 nm, an additional loss of the monomer absorption level in **2** vesicles was consistently obtained (Figure 12). If successive analyzing traces were taken[49] in the absence of laser pulsing, then the analyzing trace gradually recovered roughly to the initial absorbance level of **2** vesicles. This

(49) The analyzing light level was shown to remain stable for times corresponding to these experiments (3–4 min).

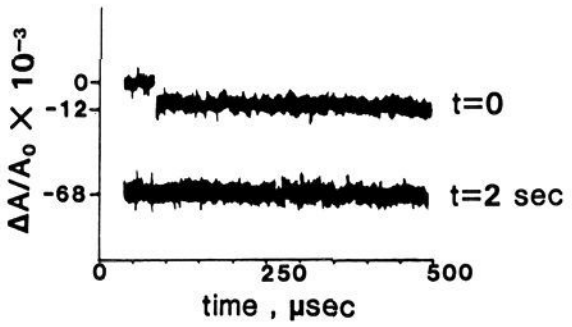

Figure 12. Depletion of absorbance, observed at 250 nm, for vesicles prepared from 1.4×10^{-4} M **2**. The top trace ($t = 0$) shows the change of monomer absorbance as a result of a single 8-mJ laser shot up to 500 μs. The lower trace ($t = 2$ s) depicts the absorbance of the same sample 2 s later.

recovery undoubtedly corresponds to the diffusion of irradiated vesicles out of the xenon lamp analyzing volume. This diffusion is not a simple phenomenon, as it depends on local heating effects, microconvection currents, and momentum transfer from the vesicle-absorbed laser photons to the vesicles themselves. Nonetheless, this experiment yielded two very valuable pieces of information. First, the fact that ground-state depletion increases over a long time (>0.5 ms <2 s) indicates that the double bonds in the styrene moiety of **2** vesicles continue to be consumed long after the photophysical events subside. This can be regarded as strong evidence for polymer chain propagation. Secondly, the 2-s to 0.5-ms ratio of ground-state depletion should yield the minimum number of monomers consumed if the original depletion is assumed to correspond to the initial free-radical population. This assumption seems to be reasonable in the light of the instant loss of monomers by triplet formation followed by a small fast depletion to a plateau value (Figure 11A) representing the population of radicalized monomers. Fairly consistent results were achieved by repeating this technique several times. Taking the mean of 13 such experiments, the average number of monomeric **2** consumed per free radicals was calculated to be 2.4 ± 0.6, giving an average polymer chain length of 3.4 ± 0.6. These values should be considered only as lower limits, since they do not allow for the diffusion of photoexcited vesicles out of the observation volume.

The extent of longer term polymerization was alternatively assessed by recording the absorption spectra of stirred vesicle samples prior and ca. 30 s subsequent to exposure to a single 8-mJ laser pulse and comparing this absorption change with that observed in flash photolysis on the 0.5-ms time scale. The laser flash photolytically observed depletion signal for this single shot on fresh **2** vesicles, monitored on an oscilloscope, averaged $\Delta C/C_0 = \Delta I \cdot (2.3)/I_0(A_0) = 0.0138$ for an 8-mJ pulse. Since the ratio of laser beam cross-sectional area to the sample cuvette is A(laser)/A(cuvette) = 0.126 cm^2/3.8 cm^2 = 0.033, the concentration change 0.5 ms after a single laser pulse in the entire sample is $0.0138 \times 0.033 = 4.55 \times 10^{-4}$. On the other hand, a much larger concentration change was observed for the same single laser pulse by the Cary spectrophotometer. $\Delta C/C_0$ values typically corresponded to 8.0×10^{-3}. Thus, the ratio of monomers consumed during chain propagation to the initial free-radical concentration averaged out to be 8.0×10^{-3}:$4.55 \times 10^{-4} = 17.6$.

If the initial slope of the long-term monomer depletion signal (Figure 11B) is taken to correspond to chain propagation in which the monomer (M) is lost according to (see Discussion, eq 34)

$$M(t) = M_0 - M_{0\cdot} - \Delta M(1 - e^{-\nu t}) \qquad (6)$$

then

$$(\mathrm{d}M/\mathrm{d}t)_{t=0} \simeq -\Delta M\nu \qquad (7)$$

where $1/\nu$ is the free-radical lifetime and ΔM is the final amount of monomers depleted through photopolymerization. Calculation of ν from eq 7 based on Figure 11B yielded $\nu = 57$ s^{-1} ± 36%. This corresponds to a free-radical lifetime of 17 ms.[50]

(50) ν is most conveniently calculated by using $\nu = (\Delta A/\Delta t)_{t=0}(M_{0\cdot}/\Delta A_0 \Delta M_f)$ where $(\Delta A/\Delta t)_{=0}$ is the slope of the presumed monomer build-down in Figure 11B, ΔA_0 is the initial-jump depletion signal in Figure 11B, and $\Delta M_f/M_0^* = 17.6$ is the number of monomers consumed per free radical.

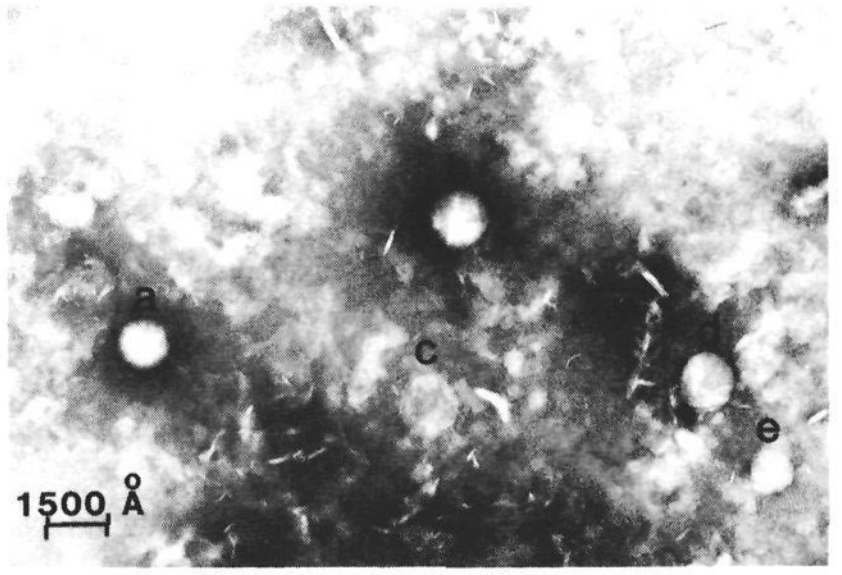

Figure 13. Electron micrographs of Xe-lamp polymerized vesicles prepared from 7×10^{-4} M **2** (D_H = 1414 Å from dynamic light scattering). See Results for details. We thank Ms. Lisa Benson for taking the electron micrographs.

Scheme I

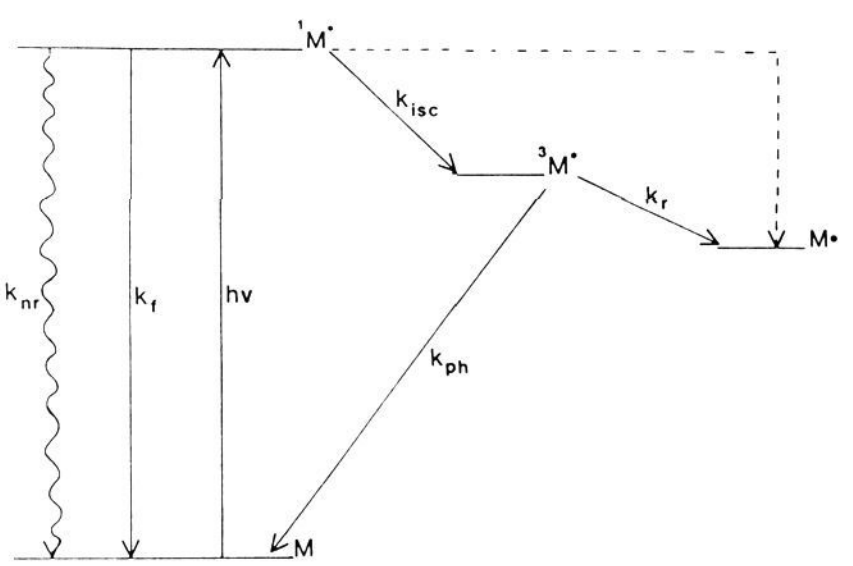

The quantum efficiency of free-radical formation, $\phi_r = M_{0\cdot}/M_0^*$ (where $M_{0\cdot}$ and M_0^* are initial free-radical and photoexcited monomer populations) was calculated from the mean of 18 depletion traces to be 0.106 ± 0.03.[51]

Electron Microscopy. Analysis of a number of electron micrographs of polymerized vesicles prepared from **2** at varying magnifications led to a mean vesicle diameter of 1450 Å. Figure 13 shows a typical electron micrograph. Five vesicles can be spotted: D_A = 1230 Å, D_B = 1436 Å, D_C = 1361 Å, D_D = 1436 Å, D_E = 1114 Å.

Fragment Analysis. Weighed amounts of freeze-dried samples of polymerized **2** were added to EtOH, MeOH, C_2Cl_4, THF, dichloroethylene, acetone, and H_2O. Light scattering exhibited low scattering intensities and large hydrodynamic radii. Typical values gave 10% of the scattering point found in vesicle solutions at the same concentration and D_H = 7000 Å. This indicates the presence of either a small population of very large aggregates, or a population of random coils of low density. In either case, none of the above systems provided a "true solvent" for the polymer.

Discussion

Polymerization in organized surfactant vesicles presents several novel aspects which do not allow the straightforward application of the theories developed for homogeneous, bulk, and emulsion polymerizations.[52,53] A simple model for vesicle photo-

(51) The quantum efficiency, Φ_r is best calculated as follows:

$$\Phi_r = M_0^*/M_0^* = (M_0^*/M_0)(M_0/M_0^*)$$

where $M_0^*/M_0 \simeq 0.0138$ at 8 mJ is calculated from the depletion traces at 250 nm, and $M_0^*/M_0 = \epsilon_{266}E = 0.13$.

(52) Ham, G. "Kinetics and Mechanisms of Polymerization"; Marcel Dekker: New York, 1967.

Scheme II

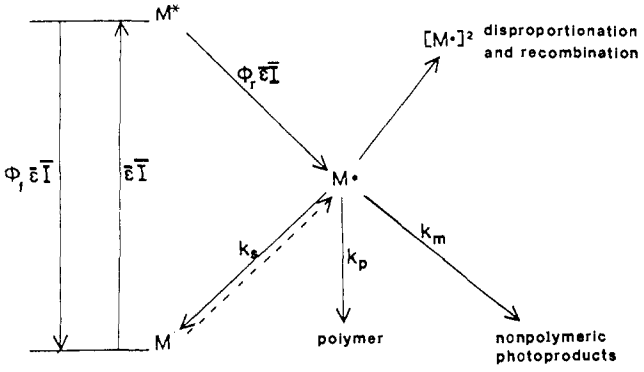

polymerization will be developed and experimentally tested. Dynamic light scattering of vesicle solutions prior and subsequent to polymerization have indicated no perceptible changes in vesicle diameters (Table I). Also, polymerization rates were found to be independent of vesicle concentrations (see below). Photopolymerization is an intravesicular process; there are virtually no vesicle–vesicle cross-linkings. It is appropriate, therefore, to model photopolymerization on a *per vesicle* rather than on a concentration or unit volume basis.

Photophysics of Radical Formation. Absorption of a photon, $h\nu$, excites the surfactant monomer, M, to its singlet excited state, $^1M^*$ (Scheme I). The majority of $^1M^*$ decays back to the ground state via fluorescence (k_f) and thermal (k_{nr}) deexcitations. Lifetimes for this process in different media are given in Table II.

Some $^1M^*$ intersystem crosses (k_{isc}) to the triplet domain, $^3M^*$. Indeed, the obtained transient absorption spectra (Figure 9) are best described in terms of styrene triplet formation.[37] A fraction of $^3M^*$ decays to the ground state via phosphorescence (k_{ph}) and the remainder interacts with another monomer or water to form a free raidcal M· by a process governed by k_r. The mechanism of styrene photolysis has been discussed in terms of free-radical formation via the triplet state. The alternative route to M· via $^1M^*$ (indicated by the dotted line in Scheme I) is less likely. The short lifetime of $^1M^*$ (Table II) precludes productive interactions with radical generating species. Lifetimes of $^3M^*$ are on the order of 100 μs. Furthermore, the greater electron separation in the triplet state than in the singlet state, as well as the electron spin alignment in the triplet state, is more favorable for chemical interactions. Conceivably, M· may also be formed by direct C–H bond scission (indicated by dotted line in Scheme II). Such a process would necessarily have an extremely small absorption cross section and is unlikely to occur to any appreciable extent. Whatever the ultimate mechanism of free-radical formation may be, it is important to stress that the equations to be developed do not depend on the way the M· is formed. Rather, their starting point is the existence of a free-radical population, $M_0\cdot$, developing virtually instantaneously from the initial excited-state population, $^1M_0^*$.

The treatment developed for photopolymerization is based on Scheme II, which does not distinguish between the separate photophysical precursors of M· (i.e., M* could be $^1M^*$ or $^3M^*$). In the scheme, Φ_f and Φ_r are respectively the quantum efficiencies for non-radical-producing excited-state depletion and for M· formation; $\bar{\epsilon}$ is the mean molecular extinction coefficient over the polymerizable absorption range (λ) expressed in cm^2 per monomer; $\bar{I}$ is the mean intensity over the polymerizable λ range, i.e., $\bar{\epsilon}\bar{I} = \int_{230\ nm}^{290\ nm} \epsilon(\gamma)L(\gamma)\,d\gamma$ where $L(\gamma)$ is the spectral irradiance of the source. Several possible fates await the free radical. Most interestingly, it can link successively to other monomers and thus propagate a polymer chain (a process governed by k_p). M· may also be deactivated and return to the ground state ("deactivation", by k_s) or react with oxygen, impurity, and the wall of the vessel (by k_m), or undergo radical disproportionations and recombinations to restore a styrene double bond and partially maintain chain propagation by conserving a free radical. This negligible term (vide infra) is represented by $[M\cdot]^2$.

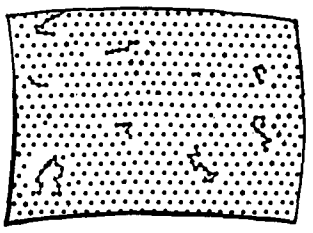

Figure 14. Schematics of multisite monomers linkages or vesicle surfactants resulting in patch polymerization.

Steady-State Photopolymerization. 1. Governing Equations. Considering photopolymerization on a *per vesicle* basis leads to the following differential equations which govern the monomers and radical consumption in steady-state photolysis:

$$dM/dt = (\Phi_f - 1)\bar{\epsilon}\bar{I}M + k_s M\cdot - k_p w(t) M\cdot + f[M\cdot]^2 \quad (8)$$

$$dM\cdot/dt = \bar{\epsilon}\bar{I}\Phi_r M - (k_m + k_s)M\cdot - (1-f)[M\cdot]^2 \quad (9)$$

$$\Phi_f + \Phi_r = 1 \quad (10)$$

$M(0) = M_0$ (initial number of monomers per vesicle is ca. 1.44×10^5) $\xrightarrow[t\to\infty]{\lim M(t)} = 0$ (11)

$$M\cdot(0) = 0 \xrightarrow[t\to\infty]{\lim M\cdot t} = 0$$

where $M(t)$ and $M\cdot(t)$ are the number, per vesicle, of double bond containing monomers remaining and free radicals present at time t, f is the fraction of free radicals involved in combinations and disproportionations which restore double-bonded monomers, and $w(t)$ indicates the average number of nearest monomeric neighbors of M at time t. Notive that propagation, $k_p w(t)M\cdot$, present only in eq 8, does not affect the M· population represented in eq 9 as the free radical is conserved upon each successful polymerization link. Notice also that the term k_m does not appear in the equation for M, as the formation of photoproduct does not restore any M.

The unique properties of vesicles require special considerations of the $f[M\cdot]^2$; $(1-f)[M\cdot]^2$, and $k_p w(t)M$ terms in eq 8 and 9. If the vesicle surface is assumed to be hexagonally packed, then each monomer is essentially in a cage constituted by its six nearest neighbors (Figure 14). The particular six neighbors of any given monomers change in time, of course, as the monomers laterally diffuse about on the vesicle surface. There is a very high probability, however, that if a free radical reacts at all it will react with one of the six nearest neighbors present at the moment of its formation. There is a rapidly decreasing probability that, if it reacts, it will react with one of the 12 nearest neighbors constituting the second layer present at its formation, or with one of the original 18 neighbors of the third layer and so on.

If A represents the number of highly probable interactive neighbors about a free radical (where $A = 6, 18, 36, \ldots, \sum_{j=1}^{m} 6j$) and m is the number of layers around a monomer considered to be highly interactive, then the probability, $P_{M\cdot M\cdot}$, that any given free radical in the total population of free radicals, $M_0\cdot$, on the vesicle surface constituted by M_0 monomers is within the interactive neighborhood of another free radical can be reasoned to be:

$$P_{M\cdot M\cdot} = \frac{A}{M_0(M_0\cdot - 1)} \sum_{n=1}^{M_0\cdot - 1} \quad (12)$$

Since $\Phi_r \simeq 0.106$ and since the numbers of photons absorbed per vesicle per second is on the order of 10^4 (vide infra) for laser polymerization, there are less than 10^3 free radicals simultaneously existing on a vesicle surface. With $M_0\cdot = 10^3$ and $M_0 = 1.4 \times$

(53) Piirma, I. "Emulsion Polymerization"; Academic Press: New York, 1982.
(54) Dorn, K.; Patton, Q. V.; Klingbiel, R. T.; O'Brien, D. F.; Ringsdorf, H. *Makromol. Chem., Rapid Commun.* **1983**, *4*, 513–517.
(55) Bolikal, D.; Regen, S. L., private communication, 1983.

10^5 in eq 12, one obtains $P_{M\cdot M\cdot} < 2.0\%$ for one interactive layer. Even for three layers $P_{M\cdot M\cdot} \sim 12\%$, and neglect, therefore, of the second-order terms, $f[M\cdot]^2$ (eq 8) and $(1-f)[M\cdot]^2$ (eq 9) is justified. In the case of steady-state photolysis it is shown later that there are less than two simultaneously existing free radicals per vesicle per second.

The polymer propagation term, $k_p w(t) M\cdot$, in eq 8, in "classical" free-radical kinetics is represented by a second-order function $k_p[M][M\cdot]$.[45] We are justified in substituting $k_p w(t) M\cdot$ for $k_p[M][M\cdot]$, since in vesicles the chain propagation is taking place in two dimensions with relatively high organization among the monomers on both the inside and outside surfaces, as contrasted to bulk and emulsion polymerizations which lack the corresponding ordering. Once a free radical has been formed on a vesicle, there is an extremely high probability of "chaining" to a nearest neighbor if it propagates prior to deactivation. Hence, the effective concentration M· sees is determined by the distribution of its nearest neighbors. Surfactant monomers on a vesicle could be considered, as a first approximation, to be hexagonally packed. Deviations could be treated as higher order dynamic perturbation terms in the expansion which would represent $\Omega(\delta_p,\delta_A,t)$, the time-dependent surface concentration, with δ_p and δ_A as the polar and azimuthal angles for monomer location on the sphere:

$$\Omega(\delta_p,\delta_A,t) = \Omega(\delta_p,\delta_A) + \Delta\Omega_0(\delta_p,\delta_A,t) \tag{13}$$

in units of monomer/area where $\Omega(\delta_p,\delta_A)$ is the equidistant distribution of the perfectly ordered vesicle.

We seek now to relate the effect the surface concentration has on monomer encounter frequency to the effect that bulk concentration has on monomer encounter frequency in homogeneous solution. Given M monomers ($\bar{M}_w = 1.0 \times 10^8$; see Table I) allows the calculation of Ω_0. For vesicles with $D_H \geq 1000$ Å, the monomers are roughly divided between the inner and outer surfaces; thus $M_0 = M/2$ is the number of monomers on either the inner or the outer vesicle surfaces. The surface concentration of monomers is

$$\Omega_0 = M_0/4\pi R^2 \tag{14}$$

and the average distance between monomers (using a hexagon to describe the area occupied by a monomer) is

$$d = (1.16/\Omega_0)^{1/2} \tag{15}$$

For monomers in bulk solution of concentration C', expressed in monomers/cm^3, where $C' = 6.02 \times 10^{20}$(monomer × liter)/(cm^3 × mole) × C, where C is the bulk concentration measured in moles/liter, we obtain $d = (1/C')^{1/3}$ for the average separation between monomers (using cubes to represent monomer occupation volumes). Using our data $d \simeq 10$ Å is calculated for the average monomer separation on the vesicle surface. A 1.5 M concentration would be required for monomers to have this average separation in bulk. In bulk polymerization the collision frequency of monomers with radicals, related to k_p, diminishes continuously towards zero with decreasing reactant concentrations. The use of $k_p[M][M\cdot]$ for the polymer chain propagation is thus appropriate. Conversely, in vesicles the concentration of M, and hence the average distance between monomers, is essentially constant (see Table I for the lack of appreciable change in vesicle diameters prior and subsequent to polymerization) so that the total number of remaining monomers on the surface has only a slight effect on chain propagation. As any polymeric chain propagates it has an increasing probability of having less than six unchained neighbors. Thus the function $w(t)$ is invoked to represent a weak function of time whose value starts at, say, 6 and very slowly goes to 0. The number of monomers left at any given time after beginning constant irradiation is a direct function of time, but the average number of neighbors that any radical will have is only weakly dependent on the total number of unchained monomers remaining on the vesicle. Thus we use a chain propagation term of the form $k_p w(t) M\cdot$. The dependence of $w(t)$ on polymerization time is so weak, in fact, that it can well be represented merely by a constant, so that the final form of the propagation term is merely $k_p M\cdot$, where k_p is now scaled by a factor equal to the time average value of $w(t)$. The slight upward deviations toward the end of the polymerization (see lines d, e, and f in Figure 5) are possibly due to $w(t)$ becoming smaller. Polymerization on vesicles is envisioned to occur in patches on the surface, so that until the polymerization is far along toward completion the majority of growing chains are independent of others. Thus $w(t)$ has even a weaker dependence on time than the foregoing effects already attributed to it. An artist's conception of patch polymerization is given in Figure 14.

2. Linearized Equations and Their Solution. With these last, well-established approximations in mind, we can now write the final form for the governing equations:

$$dM/dt = -\beta M + \gamma M\cdot \qquad \beta = \bar{\epsilon}\bar{I}\Phi_r = (1-\Phi_f)\bar{\epsilon}\bar{I} \tag{16}$$

$$\gamma = k_s - k_p$$

$$dM\cdot/dt = \beta M - \nu M\cdot \qquad \nu = k_m + k_s \tag{17}$$

Solving these simultaneous, linear equations, subject to the initial/final conditions (eq 11), we get

$$M(t) = \frac{M_0}{\rho_2 - \rho_1}[(\rho_2 + \beta)e^{\rho_1 t} - (\rho_1 + \nu)e^{\rho_2 t}] \tag{18}$$

$$M\cdot(t) = M_0\beta\left[\left(\frac{\rho_2+\beta}{\rho_2-\rho_1}\right)\left(\frac{1}{\rho_1+\nu}\right)e^{\rho_1 t} - \left(\frac{\rho_1+\beta}{\rho_2-\rho_1}\right)\left(\frac{1}{\rho_2+\nu}\right)e^{\rho_2 t}\right] \tag{19}$$

$$\rho_{1,2} = \tfrac{1}{2}\{-(\beta+\nu) \pm [(\beta+\nu)^2 - 4\beta(\nu-\gamma)]^{1/2}\} \tag{20}$$

3. Scaling Parameters to Experimental Values. While solutions 18–20 are both exact and general, they are nonetheless unwieldly for obtaining a direct idea of the polymerization process. It is convenient to simplify these solutions by scaling the terms involved to the approximate orders of magnitude in which they appear under experimental conditions by using experimental values for ϵ, $\bar{I}$, k_p, k_s, k_m, and Φ_r.

The mean molar extinction coefficient for **2** vesicles at λ 266 nm was determined to be $\epsilon = 1600$ M^{-1} cm^{-1} (see Results). Since eq 18 and 19 were derived in terms of number of monomers, it is convenient to convert ϵ to a molecular cross section by

$$\epsilon_{266nm} = 1.6 \times 10^3 \text{ M}^{-1}\text{ cm}^{-1}\text{ L} \times \frac{10^3 \text{ cm}^3}{\text{L}} \times \frac{1 \text{ mol}}{6.02 \times 10^{23} \text{ monomer}} = 2.7 \times 10^{-18} \text{ cm}^2/\text{monomer} = 0.027 \text{ Å}^2/\text{monomer} \tag{21}$$

Thus the absorption area of the monomer chromophore is quite small compared with the total area of the monomer. Likewise, for the vesicle, the total vesicular absorption cross section is simply $\epsilon = (1.4 \times 10^5$ monomer/vesicle) (0.027 Å/monomer = 3.8×10^3 Å^2), whereas the geometrical cross section of the vesicle is $\pi R^2 = 1.8 \times 10^6$ Å^2; i.e., the effective absorption cross section of the entire vesicle is only about 0.2% of the vesicle's geometrical cross section. Integrating spectral irradiance and ϵ over the range 240–350 nm yielded a value of 2×10^{-4} photons absorbed per second per monomer, which for a fresh unpolymerized vesicle yields less than 30 photons absorbed per vesicle per second.

The quantum efficiency of free-radical formation, Φ_r, was determined to be about 0.106. For xenon lamp irradiation the product $\beta = \bar{\epsilon}\bar{I}\Phi_r$ is roughly 18.0×10^{-6} photons per second per monomer, so that at any given time the number of simultaneously existing free radicals is less than 2, again showing the validity of dropping the $[M]^2$ terms in eq 8 and 9. At such low free-radical initiation rates it is appropriate to term the process "trickle polymerization".

4. Reduced Solution and Interpretation. With the approximation $\beta << \gamma, \nu$ afforded by the calculations and estimates of the last section, it is now possible to appy a binomial expansion to the solution for the exponential arguments ρ_1, ρ_2 given in eq 20.

The solution for $M(t)$, which is directly monitored by absorption measurements in the course of the experiment, is now

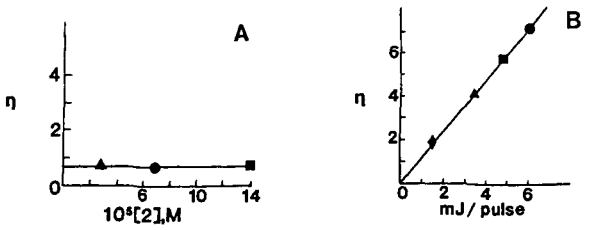

Figure 15. Plots of η values against laser energy (A) and concentration (B) for the laser-initiated polymerization of vesicles. (A) [2] = 7.0×10^{-5} (▲), 7×10^{-5} (●), 14×10^{-5} M (■). (B) Laser energy = 0.15 (♦), 0.35 (▲), 0.48 (■), and 0.6 mJ/pulse (●).

$$M(t) = (Ae^{\rho_1 t} + Be^{\rho_2 t})M_0 \tag{22}$$

where

$$A = \frac{\nu^2 + \gamma\beta - \beta\nu}{\nu^2 + 2\gamma\beta - \beta\nu} \simeq 1 - \Phi_r\bar{\epsilon}\bar{I}\frac{(k_m + k_p)}{(k_m + k_s)^2} \tag{23}$$

$$B = \frac{\beta\gamma}{\nu^2 + 2\gamma\beta - \beta\nu} \simeq \Phi_r\bar{\epsilon}\bar{I}\frac{(k_s - k_p)}{(k_m + k_s)^2} \tag{24}$$

$$\rho_1 = \beta\left(\frac{\gamma}{\nu} - 1\right) \simeq -\Phi_r\bar{\epsilon}\bar{I}\frac{(k_m + k_p)}{(k_m + k_s)} \tag{25}$$

$$\rho_2 = -\left(\nu + \frac{\gamma\beta}{\nu}\right) \simeq -(k_m + k_s) \tag{26}$$

Hence the model predicts a two-component exponential decay of monomer concentration in time for the case of steady-lamp illumination of the vesicle solution. While eq 22 refers to the number of monomers on a given vesicle, the solution is composed of a large number of vesicles (ca. 10^{15}), each polymerizing independently of the others, so that the statistical sum of this huge vesicle population should faithfully reflect the same time behavior as an average vesicle undergoing the polymerization process, for which the model equations are cast. Thus, the experimentally measured quantity, the solution monomer concentration as a function of irradiation time, [M](t), is related by a simple scale factor (the total numbers of vesicle per unit volume in the beam path of the spectrophotometer) to the model's expression for $M(t)$, the number of monomers remaining on a single average vesicle as a function of time.

If we use the estimated values of k_p, k_s, etc., from the last section, we obtain $\rho_1 = -10^{-3}$ s^{-1}, $\rho_2 = -60$ s^{-1}, $B/A < 0.02$. We see from these rough values that the amplitude of the second exponential term is much smaller than that of the first ($B < 2\%$ of A), and that its decay time $\tau_2 = 1/\rho_2 = 17 \times 10^{-3}$ s is much too fast to be measured by the technique used for the steady illumination portion of the experiment (see Experimental Section). Thus the observed monomer concentration in time should follow a single exponential decay with a characteristic decay time of $\tau_1 = 1/\rho_1 = 10^3$ s^{-1}. Indeed, the steady illumination results manifest a clear single exponential decrease with decay times on the order of 10^3 s (see Figure 4).

Before making conclusions concerning the validity of the model as evidenced by the data, however, it was necessary to consider the fact that an exponential decay could also indicate a mere photolysis or dimerization of the surface monomers. To investigate this latter possibility, solutions of **2** monomer in ethanol (not vesicles) were irradiated by both steady xenon lamp illumination, and later by laser pulses. Results show that the decay of the monomer is concentration dependent and is thus a diffusion-controlled process in bulk and not a mere pseudo-first-order photolysis of monomers. There is also a concomitant buildup of a second absorption peak in these experiments which is linked to the formation of n-mers resulting from interactions between monomers and radicalized monomers. The nonphotolytic behavior of the monomers in ethanol, together with the lack of a dimer buildup in polymerizing vesicles, is taken as further evidence for extensive polymer chain formation in the vesicles.

The decay time for the steady illumination polymerizations is directly related to the relevant photochemical parameters:

$$\tau_1 = \frac{1}{\Phi_r\bar{I}\bar{\epsilon}}\frac{(k_m + k_s)}{(k_m + k_p)} \simeq \frac{1}{\Phi_r\bar{I}\bar{\epsilon}}\frac{(k_m + k_s)}{k_p} \text{ since } k_p >> k_m \tag{27}$$

If k_m, $k_s > k_p$, then polymerized chains will not form to any appreciable degree as the free radical will usually be deactivated before propagating. Since evidence points to the formation of chains, it is safe to suppose that $k_p >> k_m$, k_s. We can write:

$$(k_s + k_m)/\Phi_r k_p \simeq \bar{\epsilon}\bar{I}\tau_1 \tag{28}$$

The average length of polymer chains will be roughly equal to the ratio of $k_p/(k_m + k_s)$, i.e., to the ratio of average free-radical deactivation time to average propagation time per polymer link. Using $\Phi_r = 0.106$, $\bar{\epsilon}\bar{I} = 2 \times 10^{-4}$, and $\tau_1 = 3600$ s, the average length of polymer chain was obtained to be 23. Because of the uncertainty in the $\bar{\epsilon}\bar{I}$ value, this number should only be considered as an order of magnitude estimate.

Pulsed Laser Photopolymerization. Taking advantage of pulsed laser photopolymerization (see Results) allowed further simplifications of the kinetic equations. The laser burst is essentially a δ function, having a full-width half-width maximum of 15 ns, after which the majority of excited monomers rapidly decay by the processes shown in Scheme I. The free-radical monomers, formed from a small portion of M, undergo the photochemical processes indicated in Scheme II. Experimental data showed the completion of all reactions within the 1 ms to 2 s time domain (see Results). Calculations indicate the probable duration of photochemistry to be about 40 ms. When the laser is used on the 2-Hz repetition rate there are 500 ms between pulses, and even longer intervals can be obtained in the single shot mode. It is safe to assume that the vesicle solutions is restored to a new equilibrium of monomers, polymers, and photoproducts prior to the arrival of the next laser pulse. As energy is now being applied in successive, essentially equal increments, the final data will be in the form of a graph of monomer concentration vs. total energy deposited, or vs. number of equi-energy laser pulses, $M(n)$, Figures 5 and 6. Without steady light illumination the governing eq 16 and 17 reduce to:

$$dM/dt = \gamma M\cdot \qquad \gamma = k_s - k_p \tag{29}$$

$$dM\cdot/dt = -\nu M\cdot \qquad \nu = k_m + k_s \tag{30}$$

with the new initial conditions:

$$M(0) = M_0 - M_0\cdot \tag{31}$$

where $M_0\cdot$ is the number of free radicals produced by the laser pulse $M_0\cdot = \Phi_r\epsilon E M_0$, E is the average energy/cm^2 of the laser pulse, calculated by dividing the measured energy per pulse by the cuvette area, M_0 is the original number of monomers on a vesicle surface, and ϵ is the molecular cross section at 266 nm. In calculating E, the relation

$$E = \frac{E_0(1 - 10^{-\epsilon Cl})}{2.3\epsilon Cl} \tag{32}$$

is used. E_0 is the laser energy passing through a blank.

Equations 29 and 30 are readily solvable and yield:

$$M\cdot(t) = M_0\cdot e^{-\nu t} \tag{33}$$

$$M(t) = M_0 - M_0\cdot + \frac{\gamma M_0\cdot}{\nu}(1 - e^{-\nu t}) \tag{34}$$

Since ν was previously determined to be about 60 s^{-1}, the time-dependent term in eq 33 decays to a steady value long before the next pulse arrives. Remembering that $k_p >> k_m$ allows the simplification:

$$\lim M(t) = M_0 - M_0\cdot + \frac{\gamma M_0\cdot}{\nu} \simeq M_0 - M_0\cdot\frac{k_p}{k_m + k_s} = M_0\left(1 - \frac{\Phi_r\epsilon E k_p}{k_m + k_s}\right) \tag{35}$$

Table III. Summary of Kinetic Parameters

quantity	symbol	value	Figure
free-radical lifetime	$1/(k_m + k_s) = 1/\nu$	17 ms ± 37%	11B
time for free-radical formation		2 μs ± 30%	11A
polymerization rate constant	k_p	1×10^3 s^{-1} ± 62%	eq 35
average polymer chain length	$k_p/(k_m + k_s)$	20 monomers ± 30%, 3.5 ± 0.5 lowest limit	12
quantum efficiency of free-radical formation	Φ_r	0.106 ± 26%	11B

It should be noted that, as expected, the greater the ratio $k_p/(k_m + k_s)$, the greater the decrease in monomer population per pulse, i.e., the bigger the polymer chains formed. It is convenient to define a quantity η, which represents the fraction of the double-bonded monomers consumed after the photochemical events induced by a single laser pulse have subsided.

$$\eta = \Phi_r \bar{\epsilon} E k_p/(k_m + k_s) \tag{36}$$

so that

$$\lim M(t) = M_0(1 - \eta) \tag{37}$$
$$t \rightarrow \text{next laser pulse}$$

If eq 36 is now taken as $M(n=1)$, then the general formula for $M(n)$, for arbitrary n, is easily induced to be:

$$M(n) = M_0(1 - \eta)^n \tag{38}$$

Taking the derivative of eq 37 leads to:

$$dM(n)/dn = \ln (1 - \eta) M(n) \tag{39}$$

Plotting $dM(n)/dn$ vs. $M(n)$ yields a straight line whose slope is equal to $\ln (1 - \eta)$. Alternatively, for small η we can use:

$$(1 - \eta)^n \simeq e^{-\eta n} \tag{40}$$

Analyzing the data both ways gives η values in excellent agreement with each other so that the analysis method chosen is one of convenience. Log curves are preferred (see Figure 5) as they offer more precision than those obtained by eq 38.

Dependence of η values on laser intensity is seen to be linear (Figure 15). More importantly, independence of η on vesicle concentration (Figure 15) substantiates the proposed mechanism of photopolymerization. The average chain length, $k_p/(k_m + k_s)$, is related to η by:

$$\frac{k_p}{k_m + k_s} = \frac{\eta}{\Phi_r \bar{\epsilon} \bar{E}} \tag{41}$$

For 1-mJ pulses $\eta = 0.00104$, and substituting values for the other constants gives 20 monomers for the average chain length. This is in good agreement with the average chain length calculated by a different procedure in the Laser Flash Photolysis section. Using this value for the chain length, we can calculate K_p: $K_p = (k_m + k_s)(\eta/\Phi_r \epsilon E) = 1 \times 10^3$ s^{-1}. The value of $(k_m + k_s)$ was calculated in the Laser Flash Photolysis section. Table III summarizes the kinetic parameters.

Summary

This work represents the first treatment of light-induced polymerization reactions in fully characterized vesicular systems. The proposed model considers the multifaceted aspects of the photophysical processes involved and provides consistent values for the degree of polymerization. Polymerization, occurring at the inner and outer surfaces, has been shown to be intravesicular. It has been analyzed, therefore, on a per vesicle basis, rather than on a volume basis as is customary in bulk or emulsion polymerizations. As a first approximation, the vesicle surface has been assumed to be hexagonally packed, each monomer, M, being surrounded by six nearest neighbor with which the initially formed free radical, M· could react. The determined hydrodynamic parameters have indicated the mean monomer–monomer separation to be approximately 10 Å, which corresponds to 1.5 M bulk concentration.

Polymerization has been envisioned to occur in patches on vesicle surfaces. Steady-state and pulsed-laser light sources have been used to initiate vesicle photopolymerizations. For steady-state illumination a single observable exponential decay of the monomer in time has been predicted and experimentally observed. Since the number of photons absorbed per vesicle per second is on the order of 10^2 at any given time for the steady-state case, photoexcitation leads to a "trickle polymerization".

Laser-induced photopolymerizations were of also predominantly monoexponential character and led to values of the percent of M lost per laser pulse (η). η values have been found to increase linearly with increasing laser intensities, but they remained constant as a function of vesicle concentration when E was corrected according to eq 32. The rate constant ratios for the laser-initiated polymerization indicated the average monomer chain length to be 20. A direct determination of polymer fragments would, however, be more informative. Recent direct determinations of polymer fragment molecular weights indicate 20 – 600 and 135 monomers per polymerized vesicles prepared from methacryloyl surfactants.[54,55] An understanding of the factors which influence the extent of surfactant vesicle cross-linking would considerably increase the potential utilization of these systems. Our efforts are directed toward obtaining such an insight.

Acknowledgment. Support of this work by the National Science Foundation and the U.S. Army Research Office is gratefully acknowledged. We thank Professor J. P. Kratohvil for his invaluable help on experiments pertaining to light scattering, NATO for a travel grant (to P.T.), and Kodak for a fellowship (to L.G.).

Registry No. 1, 88703-84-8; **2**, 88703-85-9; bis[2-(*n*-hexadecanoyloxycarbonyl)ethyl]methylamine, 88703-86-0; vinylbenzyl chloride, 30030-25-2.